Impact of solar wind fluctuations on Electric Sail mission design

Lorenzo Niccolai, Alessandro Anderlini, Giovanni Mengali, Alessandro A. Quarta*

Department of Civil and Industrial Engineering, University of Pisa, I-56122 Pisa, Italy

Abstract

The Electric Solar Wind Sail (E-sail) is a propellantless propulsion system that generates thrust by exploiting the interaction between a grid of tethers, kept at a high electric potential, and the charged particles of the solar wind. Such an advanced propulsion system allows innovative and exotic mission scenarios to be envisaged, including non-Keplerian orbits, artificial Lagrange point maintenance, and heliostationary condition attainment. In the preliminary mission analysis of an E-sail-based spacecraft, the local physical properties of the solar wind are usually specified and kept constant, while the E-sail propulsive acceleration is assumed to vary with the heliocentric distance, the sail attitude, and the grid electric voltage. However, the solar wind physical properties are known to be characterized by a marked variability, which implies a non-negligible uncertainty as to whether or not the solutions obtained with a deterministic approach are representative of the actual E-sail trajectory. The aim of this paper is to propose an effective method to evaluate the impact of solar wind variability on the E-Sail trajectory design, by considering the solar wind dynamic pressure as a random variable with a gamma distribution. In particular, the effects of plasma property fluctuations on E-sail trajectory are calculated with an uncertainty quantification procedure based on the generalized polynomial chaos method. The paper also proposes a possible control strategy that uses suitable adjustments of grid electric voltage. Numerical simulations demonstrate the importance of such a control system for missions that require a precise modulation of the propulsive acceleration magnitude.

Keywords: Electric Solar Wind Sail, solar wind fluctuations, uncertainty propagation, generalized polynomial chaos, E-sail trajectory control

Nomenclature

$\mathcal{A}$, $\mathcal{B}$	=	control strategies
$\boldsymbol{a}$	=	propulsive acceleration vector (with $a \triangleq \|\boldsymbol{a}\|$), [mm/s^2]
a_c	=	spacecraft characteristic acceleration, [mm/s^2]
f	=	probability density function
L	=	tether length, [km]
L_1	=	collinear Lagrange point
M	=	dimension of vector $\boldsymbol{\xi}$
m	=	spacecraft mass, [kg]
N	=	number of tethers
$\hat{\boldsymbol{n}}$	=	unit vector normal to the E-sail nominal plane
P	=	truncation order of Eq. (8)
p	=	solar wind dynamic pressure, [nPa]
R	=	generic random process, see Eq. (8)

*Corresponding author

Email addresses: lorenzo.niccolai@ing.unipi.it (Lorenzo Niccolai), alessandro.anderlini@ing.unipi.it (Alessandro Anderlini), g.mengali@ing.unipi.it (Giovanni Mengali), a.quarta@ing.unipi.it (Alessandro A. Quarta)

Published in Aerospace Science and Technology, Vol. 82–83, November 2018, pp. 38–45. doi: https://doi.org/10.1016/j.ast.2018.08.032

$\boldsymbol{r}$	=	position vector (with $r \triangleq \|\boldsymbol{r}\|$), [au]
T	=	total flight time, [days]
t	=	time, [days]
V	=	grid electric voltage, [kV]
w	=	weighting function
V_w	=	solar wind electric potential, [kV]
$\boldsymbol{v}$	=	spacecraft orbital velocity vector, [km/s]
α	=	shape parameter of the gamma distribution
β	=	scale parameter of the gamma distribution
Γ	=	gamma function
ϵ	=	dimensionless tolerance
ϵ_0	=	vacuum permittivity, [F/m]
λ	=	projection coefficient, see Eq. (10)
$\mu_\odot$	=	Sun's gravitational parameter, [$\mathrm{km}^3/\mathrm{s}^2$]
$\mu_\oplus$	=	Earth's gravitational parameter, [$\mathrm{km}^3/\mathrm{s}^2$]
$\boldsymbol{\xi}$	=	random vector of uncertainty parameters
ρ	=	radial error, [au]
σ	=	tether maximum thrust magnitude per unit length, [N/m]
τ	=	switching parameter
Ψ	=	polynomial base
Ω	=	parameter space

Subscripts

0	=	initial conditions
gPC	=	generalized Polynomial Chaos
H	=	heliostationary condition
h	=	generic time step
j	=	polynomial base index
L	=	artificial Lagrange point
max	=	maximum allowable value
req	=	required value
st	=	maximum step variation
$\oplus$	=	value at $r = 1\,\mathrm{au}$

Superscripts

$-$	=	mean or nominal value
$\cdot$	=	time derivative
$\widehat{\ }$	=	unit vector

1. Introduction

The Electric Solar Wind Sail (E-sail) is a propellantless propulsion system that exploits the interaction of the charged particles in the solar wind with a spinning grid of tethers, kept at high potential by an electron gun and stretched by the centrifugal force [1, 2, 3]. The peculiarity of an E-sail allows innovative and exotic mission scenarios to be feasible, including non-Keplerian orbits and artificial Lagrange points maintenance [4, 5, 6]. An in-situ test of the E-sail technology has not been performed yet, even though the lack of experimental data should be overcome by Aalto-1 satellite [7], which is scheduled to validate the plasma brake technology [8, 9], a derivation of the E-sail concept for spacecraft deorbiting in a planetocentric mission.

The analysis of E-sail trajectories in a preliminary mission phase is usually addressed within a deterministic approach and, in this respect, analytical models exist for estimating the thrust vector [10, 11, 12, 13] as a function of the E-sail design parameters. The local characteristics of the solar wind, such as plasma

number density and particle velocity, are taken as constant parameters in Refs. [10, 11, 12, 13], which corresponds to assuming a fixed value of the local solar wind dynamic pressure. Under this hypothesis, the E-sail propulsive acceleration vector is a function of the Sun-spacecraft distance, the sail attitude, and the grid electric voltage, so that the spacecraft trajectory may be obtained by simple numerical integration of the differential equations of motion. However, the assumption of constant local properties of the plasma is at odd with data on solar wind characteristics obtained by a number of space missions, such as Voyager 2 [14], Ulysses [15], and ACE [16]. Indeed, the in-situ measurements of plasma density, bulk speed, and dynamic pressure exhibit a chaotic and unpredictable behaviour, with time fluctuations comparable to their mean value [17, 18, 19, 20]. For these reasons, a refined mission analysis requires the solar wind dynamic pressure for E-sail thrust generation to be described with more realistic models [21, 22, 23]. The aim of this work is to propose an effective method to evaluate the impact of the solar wind variability on E-Sail interplanetary trajectories, and propose a control strategy that counteracts the solar wind-induced perturbations by adjusting the grid electric voltage. In particular, the solar wind dynamic pressure is modelled as a random variable with a gamma distribution, and its effects on the E-sail trajectories are simulated with stochastic methods [24].

Loosely speaking, a stochastic approach refers to a group of different mathematical algorithms capable of quantifying how the uncertainty on a set of design parameters, modelled as random variables with a given Probability Density Function (PDF), propagates into a complex model. From a practical standpoint, a continuous response surface of a given performance index in the parameter space may be approximated at a computationally inexpensive cost with a reduced number of deterministic evaluations.

In this work, a method based on generalized Polynomial Chaos (gPC) [25] is used to generate the response surface of the Sun-spacecraft distance as a function of the solar wind dynamic pressure. A gPC is a spectral projection over a known orthogonal polynomial base, whose result is a sum of polynomials with suitable coefficients that are evaluated through inner products. Due to its generality, such an approach has been used in the last years for both aeronautical [26] and aerospace [24] applications.

The paper is organized as follows. The recent E-sail thrust model is first briefly summarized. The plasma dynamic pressure is modelled as a random variable with a suitable PDF, based on available solar wind real data. A gPC-based methodology is then used to analyze the effect of the solar wind variability on the E-Sail trajectory, showing that the assumption of a fixed value of the local solar wind dynamic pressure may produce inaccurate results even for short flight times. A control strategy is therefore discussed for overcoming such a problem, where the solar wind-induced perturbations are balanced by suitably adjusting the grid electric voltage. The effectiveness of the proposed a control law is illustrated by simulating two advanced mission scenarios. The main outcomes of the work are finally highlighted.

2. Mathematical model

Consider an E-sail-based spacecraft, placed at distance $r = r_\oplus \triangleq 1\,\text{au}$ from the Sun. The spacecraft equations of motion in a heliocentric-ecliptic (inertial) reference frame are

$$\dot{\boldsymbol{r}} = \boldsymbol{v} \tag{1}$$

$$\dot{\boldsymbol{v}} = -\frac{\mu_\odot}{r^3}\,\boldsymbol{r} + \boldsymbol{a} \tag{2}$$

where $\boldsymbol{r}$ is the spacecraft position vector (with $r \triangleq \|\boldsymbol{r}\|$), $\boldsymbol{v}$ is the velocity vector, $\mu_\odot$ is the Sun's gravitational parameter, and $\boldsymbol{a}$ is the propulsive acceleration vector. To a first order approximation the E-sail shape is modelled as a disk, and its propulsive acceleration vector is written as [12]

$$\boldsymbol{a} = \tau\,\frac{a_c}{2}\,\left(\frac{r_\oplus}{r}\right)\,[\hat{\boldsymbol{r}} + (\hat{\boldsymbol{r}}\cdot\hat{\boldsymbol{n}})\,\hat{\boldsymbol{n}}] \tag{3}$$

where $\tau \in \{0, 1\}$ is a switching parameter that accounts for the possibility of switching either off ($\tau = 0$) or on ($\tau = 1$) the E-sail electron gun, $\hat{\boldsymbol{r}} = \boldsymbol{r}/r$ is the Sun-spacecraft unit vector, $\hat{\boldsymbol{n}}$ is the unit vector normal to the sail nominal plane in the direction opposite to the Sun, and a_c is the spacecraft characteristic acceleration, defined as the maximum propulsive acceleration at $r = r_\oplus$, see Fig. 1. As implied by Eq. (3), the propulsive acceleration of a flat E-sail depends on its spacecraft attitude, that is, on the orientation of

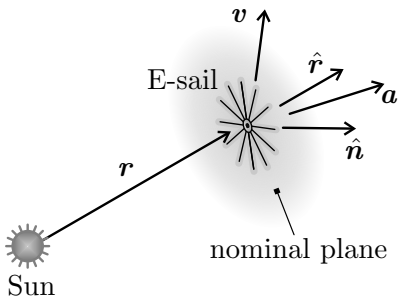

Figure 1: E-sail conceptual scheme.

the sail plane with respect to the radial direction. Notably, the same Eq. (3) may also be used to characterize the acceleration of a three-dimensional sail, provided its shape is modelled as an axially symmetric body, which spins around the Sun-spacecraft line and has a Sun-facing orientation, that is, $\hat{\boldsymbol{r}} \equiv \hat{\boldsymbol{n}}$ [13].

2.1. E-sail performance parameter

The typical E-sail performance parameter in the preliminary mission phase is the spacecraft characteristic acceleration a_c. Its value is usually assumed to remain constant along the whole spacecraft trajectory [27, 28, 29], and is written as [12]

$$a_c = \frac{N\,L\,\sigma_\oplus}{m} \tag{4}$$

where N is the number of tethers, L is the (generic) tether length, m is the total spacecraft mass, and $\sigma_\oplus$ is given by [10, 30]

$$\sigma_\oplus \triangleq 0.18\,\max\left(0,\, V - V_\mathrm{w}\right)\sqrt{\epsilon_0\, p_\oplus} \tag{5}$$

in which V_w is the electric potential of the solar wind ions (with a typical value of about 1 kV), V is the grid electric voltage (with a typical value of a few tens of kilovolts), ϵ_0 is the vacuum permittivity, and $p_\oplus$ is the solar wind dynamic pressure at $r = r_\oplus$. Note that $\sigma_\oplus$ can been thought of as the maximum thrust per unit length generated by a tether at a distance $r = r_\oplus$ from the Sun. Assuming $V \gg V_\mathrm{w}$ in Eq. (5), the characteristic acceleration (4) may be conveniently approximated as

$$a_c \simeq \frac{0.18\,N\,L\,V}{m}\sqrt{\epsilon_0\, p_\oplus} \tag{6}$$

In a preliminary mission analysis phase, the solar wind dynamic pressure $p_\oplus$ is typically assumed to take the same value at each heliocentric latitude and at any time instant. In fact, a constant value of $\{p_\oplus, V\}$ corresponds to a constant value of a_c throughout the flight, see Eq. (6). According to Refs. [15, 31], the hypothesis of latitude-invariance for $p_\oplus$ is sufficiently accurate, provided the heliocentric latitude of the spacecraft does not have substantial variations during the mission. In other terms, as long as the analysis is confined to trajectories with moderate inclinations relative to the ecliptic plane (or displaced non-Keplerian orbits of constant latitude), the assumption of latitude-invariance of the solar wind dynamic pressure $p_\oplus$ is consistent with the solar wind behaviour. However, at a given heliocentric latitude, the value of $p_\oplus$ undergoes significant time fluctuations, comparable to its mean value [15]. An example of hourly variation of the solar wind dynamic pressure $p_\oplus$ on the ecliptic plane is shown in Fig. 2, for a time-span ranging from January 1996 to September 2013, according to the data reported by NASA[1]. Even though it is possible to recognize a weak periodicity related to the 11-year solar activity cycle, the solar wind time fluctuations are highly irregular and unpredictable and take place in short time intervals, on the order of a few hours. As a result, in a refined mission analysis phase, the value of a_c may be hardly taken as constant, as implied by Eq. (6). The local value of $p_\oplus$ is now therefore modelled as a random variable, to obtain more reliable information on the actual spacecraft characteristic acceleration and, as such, on the propulsive acceleration vector given by Eq. (3).

[1]See `https://omniweb.gsfc.nasa.gov/form/dx1.html`. Retrieved on May 22, 2018.

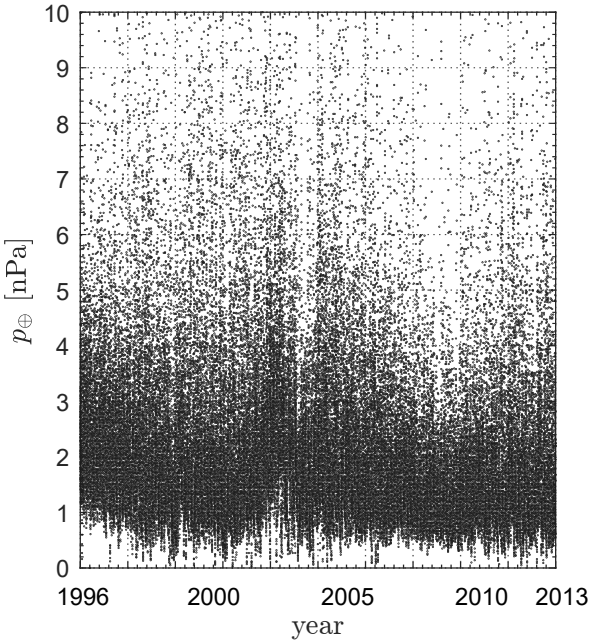

Figure 2: Hourly in-situ measurements of $p_\oplus$ from January 1996 to September 2013. Data taken from NASA.

2.2. Statistical evaluation of solar wind dynamic pressure

To describe the solar wind (local) fluctuations, the dynamic pressure $p_\oplus$ is modelled as a random variable whose instantaneous value is unaffected by the previous ones [18]. In other terms, this corresponds to neglecting the periodic variations due to the solar activity cycles. Note that such an assumption is conservative, since it overestimates the unpredictability of solar wind properties, and makes the succeeding design of a control strategy based on the electric voltage variation more difficult. Figure 3 shows the histogram plot of the PDF of the values of $p_\oplus$ reported in Fig. 2. Note the existence of a significant asymmetry, with a mean value of $\overline{p}_\oplus = 2\,\mathrm{nPa}$ and a standard deviation of 1.56 nPa, see Fig. 3. These data are relative to a large time-span (almost 18 years), and no significant periodic behaviour is evident. Accordingly, the hypothesis that each value of $p_\oplus$ is unaffected by the previous ones seems to be fairly realistic, since relevant variations take place even in a few hours, see Fig. 2.

The measurements reported in Fig. 3 may be reasonably approximated with a PDF in the form of a gamma distribution

$$f(p_\oplus) = \frac{\beta^{-\alpha}}{\Gamma(\alpha)}\, p_\oplus^{\alpha-1}\, \exp\left(-p_\oplus/\beta\right) \tag{7}$$

where $f(p_\oplus)\,\mathrm{d}p_\oplus$ is the probability that the dynamic pressure at a distance $r_\oplus$ from the Sun ranges between $p_\oplus$ and $p_\oplus + \mathrm{d}p_\oplus$, $\Gamma(x)$ denotes the gamma function of the variable x, whereas α and β are the two parameters necessary to define the properties of the PDF. In particular, the mean value and standard deviation of the data reported in Fig. 3 are suitably fitted with $\alpha = 1.6437$ and $\beta = 1.2168$. The assumption of a PDF in the form of Eq. (7) implies that the higher-order statistical moments cannot be freely assigned as they depend on α and β. In practice, the skewness and the kurtosis indexes are both underestimated. However, the accordance between the gamma distribution and the experimental data, see Figs. 3 and 4, is sufficient for appreciating the impact of solar wind fluctuations on the E-sail trajectory.

2.3. gPC-based procedure

A gPC-based procedure [25] is used to quantify how the uncertainty on the dynamic pressure propagates into the spacecraft dynamics and, in particular, in the Sun-spacecraft distance r. The non-intrusive gPC is

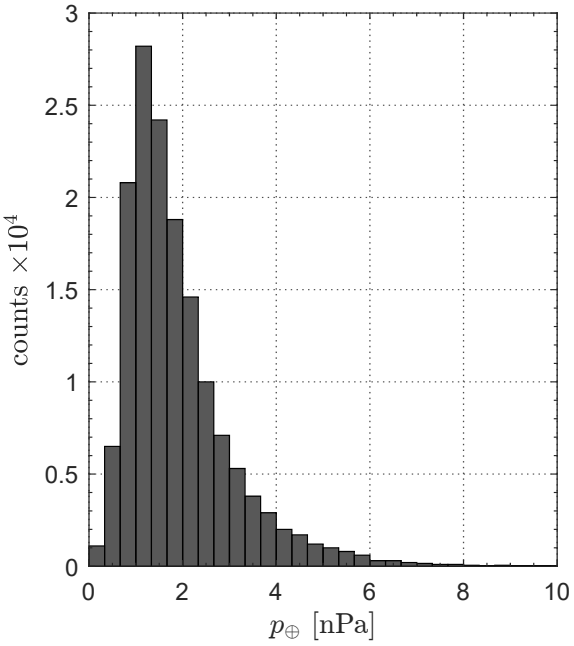

Figure 3: PDF of $p_\oplus$ from January 1996 to September 2013. Data taken from NASA.

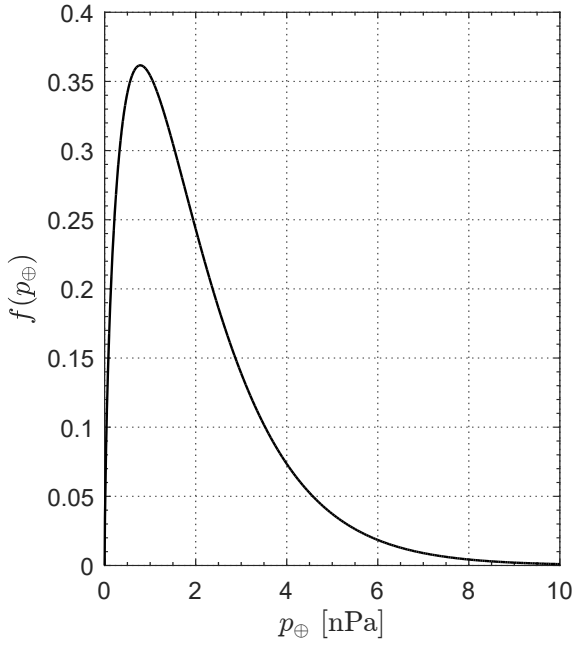

Figure 4: Gamma distribution of $p_\oplus$, see Eq. (7).

a projection of a random process R over a known orthogonal polynomial base, which can be expressed as

$$R = \sum_{j=0}^{\infty} \lambda_j \, \Psi_j(\boldsymbol{\xi}) \tag{8}$$

where $\boldsymbol{\xi}$ is a random vector of dimension M, belonging to the parameter space Ω, whose components are the uncertain parameters. In addition, $\Psi_j(\boldsymbol{\xi})$ is the gPC polynomial base of index j, while λ_j is the corresponding projection coefficient. For practical purposes, the series in Eq. (8) is truncated at order P, viz.

$$R_{\mathrm{gPC}} = \sum_{j=0}^{P} \lambda_j \, \Psi_j(\boldsymbol{\xi}) \tag{9}$$

Due to the orthogonality property of polynomials, the coefficients λ_j are obtained as

$$\lambda_j = \frac{\langle R, \Psi_j \rangle}{\langle \Psi_j, \Psi_j \rangle} \tag{10}$$

where $\langle g, u \rangle$ denotes the inner product between two generic functions g and u. In particular, in the scalar case ($M = 1$), the inner product is defined as

$$\langle g, u \rangle = \int_{\Omega} w(\xi) \, g(\xi) \, u(\xi) \, \mathrm{d}\xi \tag{11}$$

Note that g and u are multiplied by a weighting function w, which is the PDF of the random variable ξ. Since the polynomials are orthogonal to the weighting function, the choice of the polynomial family depends on the input parameter distribution. In particular, for a gamma distribution, the set of generalized Gauss-Laguerre polynomials is used. A single uncertain parameter is assumed, that is $\xi \equiv p_{\oplus}$, and the summation (9) is truncated at $P = 4$. The inner products are calculated with a Gaussian Quadrature Formula using $(P + 1) = 5$ quadrature points. Each quadrature point defines a node where the process R is sampled, so that $(P + 1)$ deterministic evaluations only are sufficient to propagate the uncertainty in the dynamic model.

2.4. Test case

The above-described procedure has been used to perform a stochastic simulation of the heliocentric trajectory of an E-sail-based spacecraft that initially covers a circular orbit of radius $r = r_{\oplus}$. This example models a spacecraft that escapes from the Earth's gravitational field using a parabolic orbit with respect to the planet. The electron gun is assumed to be always switched on ($\tau = 1$), and the E-sail is maintained at a Sun-facing attitude ($\hat{\boldsymbol{n}} = \hat{\boldsymbol{r}}$) with a constant value of the grid electric voltage. Note that for a Sun-facing sail, the (local) propulsive acceleration magnitude takes its maximum value, see Eq. (3). The selected nominal value (denoted by an over-bar symbol) of the spacecraft characteristic acceleration is consistent with a near-term technology level in E-sail design [32]. Such a characteristic acceleration corresponds to an E-sail based spacecraft with $m = 560\,\mathrm{kg}$, $N = 24$, $V = 25\,\mathrm{kV}$, $L \simeq 8\,\mathrm{km}$, and $p_{\oplus} = 2\,\mathrm{nPa}$, see Eq. (6). In particular, the nominal characteristic acceleration $\overline{a}_c = 0.2\,\mathrm{mm/s^2}$ corresponds to an ideal situation of solar wind dynamic pressure $p_{\oplus}$ constant and equal to its mean value $\overline{p}_{\oplus} = 2\,\mathrm{nPa}$. The effect of a solar wind uncertainty on the E-Sail trajectory, that is, the impact of the variability of $p_{\oplus}$ on the Sun-spacecraft distance, can be evaluated by analyzing the heliocentric polar trajectory dispersion for $\theta \in [0, 180]\,\mathrm{deg}$, where θ is the spacecraft polar angle measured counterclockwise from its initial position vector direction. Figure 5 shows the PDF distribution (normalized with respect to its peak value) of $r = r(\theta)$, where dark lines represent highly probable spacecraft trajectories.

Note that the spacecraft position has a non-negligible uncertainty after just one half revolution around the Sun ($\theta = 180\,\mathrm{deg}$), even when the spacecraft attitude is fixed with respect to an orbital reference frame (Sun-facing case). This may constitute a significant issue for missions requiring an accurate estimate of the thrust vector such as, for example, interplanetary rendez-vous [27] or generation of highly non-Keplerian orbits [4, 5, 6]. In these cases a suitable control system, capable of adjusting the propulsive acceleration magnitude as a function of the instantaneous solar wind characteristics is therefore advisable, as is discussed in the next section.

3. E-sail control strategies

Two possible control algorithms that may be used by an E-sail-based spacecraft to track a nominal trajectory are now proposed. In so doing, the only control variable to be selected by the guidance system is

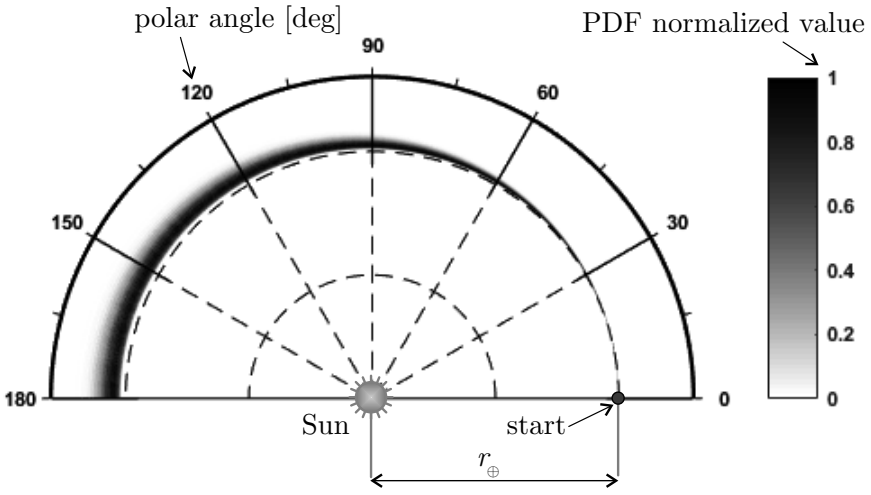

Figure 5: Normalized PDF distribution of the Sun-spacecraft distance for a Sun-facing sail with $\overline{a}_c = 0.2\,\mathrm{mm/s^2}$.

the grid electric voltage [10, 22, 30]. In fact, the sail attitude (that is, the unit vector $\hat{\boldsymbol{n}}$) must be adjusted so as to obtain the desired thrust direction, while the other variables involved in the thrust generation depend on the Sun-spacecraft distance and on the environmental conditions, see Eq. (6). In this preliminary analysis, it is assumed that the power consumption of the electron gun can be slightly varied. This hypothesis has a limited impact on the discussed simulations as it does not significantly affect the propulsive acceleration generated by the E-sail. Indeed, the power consumption can be estimated by the orbital motion limited (OML) current collection theory, according to which it is proportional to both the plasma number density and $V^{3/2}$ [27, 33]. A hypothetical constraint of constant power consumption would imply a voltage reduction when the plasma number density (and, consequently, the dynamic pressure) increases, with a resultant very small variation in the generated thrust.

3.1. Dynamic pressure-based control law

The first proposed strategy is to adjust the grid electric voltage V in response to the measured value of the (local) solar wind dynamic pressure $p(t) = p_\oplus(t)\ (r_\oplus/r)^2$, in such a way that the spacecraft characteristic acceleration fits the nominal value given by

$$\overline{a}_c = \frac{0.18\,N\,L\,\overline{V}}{m}\,\sqrt{\epsilon_0\,\overline{p}_\oplus} \tag{12}$$

where $\overline{V}$ is the nominal grid electric voltage, see Eq. (6).

It is assumed that the spacecraft is equipped with a sensor capable of measuring the instantaneous value of the solar wind dynamic pressure, such as a particle detector. In case the shielding action due to the charged grid is very large and makes the sensor ineffective, the latter could be replaced by an accelerometer that measures the instantaneous generated thrust, from which the dynamic pressure can be calculated through Eq. (6). The required value of the grid electric voltage $V_{\mathrm{req}}(t)$ is found from Eq. (4) as

$$V_{\mathrm{req}}(t) \triangleq \frac{m\,\overline{a}_c}{0.18\,N\,L\,\sqrt{\epsilon_0\,p_\oplus(t)}} \equiv \overline{V}\,\sqrt{\frac{\overline{p}_\oplus}{p_\oplus(t)}} \tag{13}$$

If the control system were capable of modifying the grid electric voltage with no delay and without any voltage limitations, the nominal trajectory could be tracked by simply enforcing $V(t) = V_{\mathrm{req}}(t)$ for all $t \geq t_0 \triangleq 0$. However, the grid electric voltage V is constrained by a maximum value $V_{\max}$, and may only be continuously modified by a certain amount $\Delta V \leq V_{\mathrm{st}}$ with $V_{\mathrm{st}} \in [0,\, V_{\max}]$ [21]. Therefore, assuming the mission to be divided into legs within which the voltage is kept constant, the E-sail voltage $V(t_h)$, at a

generic time t_h where a leg starts, is a function not only of the solar wind properties through $p(t)$, but also of $\{V_{\max}, V_{\mathrm{st}}\}$ and of the previous value $V(t_{h-1})$, that is

$$V(t_h) = \begin{cases} V(t_{h-1}) - V_{\mathrm{st}} & \text{if} \quad V_{\mathrm{req}}(t_h) < V(t_{h-1}) - V_{\mathrm{st}} \\ V_{\mathrm{req}}(t_h) & \text{if} \quad V_{\mathrm{req}}(t_h) \in [V(t_{h-1}) - V_{\mathrm{st}},\, V(t_{h-1}) + V_{\mathrm{st}}] \\ V(t_{h-1}) + V_{\mathrm{st}} & \text{if} \quad V_{\mathrm{req}}(t_h) > V(t_{h-1}) + V_{\mathrm{st}} \quad \text{and} \quad V(t_{h-1}) + V_{\mathrm{st}} \leq V_{\max} \\ V_{\max} & \text{if} \quad V_{\mathrm{req}}(t_h) > V(t_{h-1}) + V_{\mathrm{st}} \quad \text{and} \quad V(t_{h-1}) + V_{\mathrm{st}} > V_{\max} \end{cases} \tag{14}$$

The staircase control law described by Eq. (14) is initialized by assuming that the E-sail is turned on at t_0 with a voltage equal to the nominal value $V(t_0) = \overline{V}$. The control law of Eq. (14) will be referred to as control strategy $\mathcal{A}$ in the rest of the work.

3.2. Heliocentric distance-based control law

Another control strategy consists in relating the grid electric voltage with the Sun-spacecraft distance, provided the spacecraft is able to accurately determining the value of $r(t)$. In this case, at the initial time of each leg the spacecraft measures the instantaneous Sun-spacecraft distance $r(t_h)$, which is compared by the onboard guidance system with the desired, nominal, value $\overline{r}(t)$.

The control strategy consists in increasing (decreasing) the grid electric voltage when $r(t_h)$ is smaller (greater) than the nominal value $\overline{r}(t_h)$, that is

$$V(t_h) = \begin{cases} V_{\max} & \text{if} \quad r(t_h) < \overline{r}(t_h)(1-\epsilon) \quad \text{and} \quad V(t_{h-1}) + V_{\mathrm{st}} > V_{\max} \\ V(t_{h-1}) + V_{\mathrm{st}} & \text{if} \quad r(t_h) < \overline{r}(t_h)(1-\epsilon) \quad \text{and} \quad V(t_{h-1}) + V_{\mathrm{st}} \leq V_{\max} \\ V(t_{h-1}) & \text{if} \quad \dfrac{|r(t_h) - \overline{r}(t_h)|}{\overline{r}(t_h)} \leq \epsilon \\ V(t_{h-1}) - V_{\mathrm{st}} & \text{if} \quad r(t_h) > \overline{r}(t_h)(1+\epsilon) \quad \text{and} \quad V(t_{h-1}) \geq V_{\mathrm{st}} \\ 0 & \text{if} \quad r(t_h) > \overline{r}(t_h)(1+\epsilon) \quad \text{and} \quad V(t_{h-1}) < V_{\mathrm{st}} \end{cases} \tag{15}$$

where ϵ is a given small dimensionless parameter (tolerance). The control law reassumed by Eq. (15) is denoted with the symbol $\mathcal{B}$ and is initialized by $V(t_0) = \overline{V}$. Note that Eq. (15) accounts for a grid electric voltage that may take a finite number of values only, thus offering a possible simplification of the power system design.

4. Mission applications

The previous control algorithms $\mathcal{A}$ and $\mathcal{B}$ are now simulated in two advanced mission scenarios, in order to investigate their performance in maintaining a working orbit that requires an accurate thrust vector modulation for a long time interval.

4.1. Heliostationary condition generation

An interesting, albeit exotic, mission application for an E-sail-based spacecraft is the generation of a heliostationary condition [34, 35], characterized by a spacecraft that maintains a fixed position with respect to an inertial reference frame, as illustrated in Fig. 6. When the spacecraft has reached the heliostationary point, the propulsive acceleration given by a Sun-facing E-sail is used to balance the Sun's gravitational pull. This mission scenario has interesting scientific implications such as, for example, the observation of the Sun's polar region by a vantage point, the monitoring of near-Earth objects, or the release of a small solar probe along a rectilinear trajectory [36, 37]. Note that the assumption of small variation of the heliocentric latitude is consistent with this mission scenario, since a spacecraft in a heliostationary condition maintains a time-invariant position with respect to the Sun.

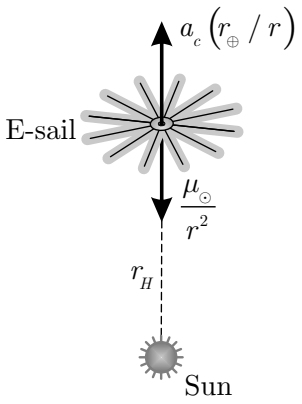

Figure 6: Sketch of the heliostationary condition.

The Sun-spacecraft heliostationary distance r_H and the required (nominal) characteristic acceleration $\overline{a}_c$ are obtained by enforcing the balance between the Sun's gravitational pull and the Sun-facing E-sail thrust (see Fig. 6), calculated from Eq. (3) with $\tau = 1$ (electron gun switched on) and $\hat{\boldsymbol{n}} = \hat{\boldsymbol{r}}$, viz.

$$\frac{\mu_\odot}{r_H^2} = \overline{a}_c \left(\frac{r_\oplus}{r_H}\right) \tag{16}$$

For a given value of r_H, the nominal characteristic acceleration $\overline{a}_c$ required to maintain the heliostationary condition is therefore

$$\overline{a}_c = \frac{\mu_\odot}{r_\oplus\, r_H} \tag{17}$$

When $r_H = r_\oplus = 1\,\mathrm{au}$, the (required) nominal characteristic acceleration given by Eq. (17) is $\overline{a}_c = \mu_\odot / r_\oplus^2 \simeq 5.93\,\mathrm{mm/s^2}$, a value corresponding to a high-performance E-sail.

Assuming that the total simulation time of $T = 0.25\,\mathrm{year}$ is divided into legs of about $1\,\mathrm{year}/(2\pi \times 100) \simeq 0.58\,\mathrm{days}$, Tables 1 and 2 report the radial error, defined as

$$\rho_H(t) \triangleq |r(t) - r_H| \tag{18}$$

for the two control strategies as a function of $\{V_{\max}, V_{\mathrm{st}}, \epsilon\}$. For each triplet, 100 simulations have been conducted as follows. At the beginning of each leg, the solar wind dynamic pressure is generated as a random variable with a PDF in the form of Eq. (7), and the grid electric voltage is adjusted according to the control law $\mathcal{A}$, see Eq. (14), or $\mathcal{B}$, see Eq. (15). The equations of motion are integrated in double precision using a variable order Adams-Bashforth-Moulton solver scheme [38, 39] with absolute and relative errors of 10^{-12} until the end of the leg, when a new value of the dynamic pressure is generated and the procedure is restarted, up to the final time T is reached.

Table 2 shows that a smallest value of the tolerance ϵ gives better performance, but the control law $\mathcal{A}$ significantly outperforms the control law $\mathcal{B}$. However, note that an accurate position maintenance is possible only for large values of both $V_{\max}$ and V_{st}, even for a short mission time of about 3 months only.

4.2. Artificial Lagrange point maintenance

The second mission scenario consists in the generation of a L_1-type artificial (collinear) Lagrange point in the Sun-[Earth+Moon] three-body system [40, 41, 42], at a distance r_L from the Sun. In particular, r_L is chosen to be less than the actual Sun-L_1 distance, that is, less than 0.99 au, see Fig. 7. Such a mission is important for solar observation purposes, since when placed in the artificial point, the spacecraft would be able to provide an early warning in the event of coronal mass ejections or solar flares [6], thus representing an improvement with respect to the ACE mission [16], which covers a Halo orbit around the Sun-Earth L_1 point, with a warning time capability of about 1 hour.

$V_{\max}$ [kV]	V_{st} [kV]	ρ_H [au]		ρ_H/r_H [%]	
		mean	max	mean	max
40	1	0.0170	0.1442	1.699	14.418
	5	0.0123	0.1123	1.227	11.227
	10	0.0111	0.0981	1.138	9.807
	40	0.0265	0.1427	2.655	14.266
60	1	0.0176	0.2499	1.758	24.986
	5	0.0109	0.1338	1.086	13.377
	10	0.0114	0.1277	1.1405	12.767
	60	0.0076	0.0543	0.763	5.428
80	1	0.0185	0.1492	1.854	14.915
	5	0.0132	0.1293	1.320	12.933
	10	0.0091	0.0838	0.907	8.377
	80	0.0035	0.0291	0.3478	2.906
no control		0.0387	0.2538	3.868	25.381

Table 1: Results of the simulations for the heliostationary condition (control strategy $\mathcal{A}$).

$V_{\max}$ [kV]	V_{st} [kV]	ϵ	ρ_H [au]		ρ_H/r_H [%]	
			mean	max	mean	max
40	5	0	0.0139	0.0748	1.388	7.483
		0.01	0.0487	0.1736	4.871	17.361
	10	0	0.0082	0.0437	0.823	4.373
		0.01	0.0412	0.1581	4.124	15.811
60	5	0	0.0306	0.1423	3.062	14.234
		0.01	0.0683	0.1927	6.826	19.268
	10	0	0.0161	0.0851	1.609	8.506
		0.01	0.0392	0.1405	3.920	14.054
80	5	0	0.0450	0.2533	4.495	25.333
		0.01	0.1345	0.4135	13.451	41.349
	10	0	0.0292	0.1411	2.925	14.107
		0.01	0.0808	0.2661	8.077	26.606
no control			0.0387	0.2538	3.868	25.381

Table 2: Results of the simulations for the heliostationary condition (control strategy $\mathcal{B}$)

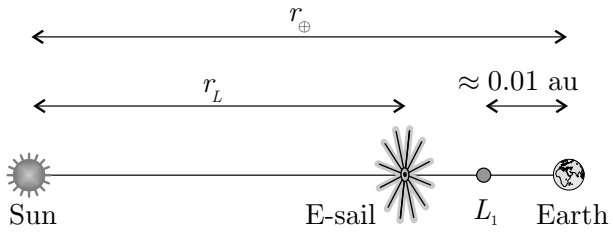

Figure 7: Sketch of the artificial (collinear) Lagrangian point maintenance.

In this case, the spacecraft heliocentric trajectory is a nearly circular non-Keplerian orbit, with a radius of $r = r_L$ and a period of 1 year, such that the Sun, the spacecraft, and the Earth are always aligned. The artificial Lagrange point may be maintained using the continuous propulsive acceleration generated by a Sun-facing E-sail [4]. The value of r_L is found by enforcing an equilibrium condition between the Sun's and

Earth's gravitational pulls, the propulsive acceleration, and the centrifugal acceleration [41], viz.

$$-\frac{\mu_{\odot}}{r_L^2}+\frac{\mu_{\oplus}}{(r_{\oplus}-r_L)^2}+\overline{a}_c\left(\frac{r_{\oplus}}{r_L}\right)+\frac{\mu_{\odot}}{r_{\oplus}^3}\,r_L=0 \tag{19}$$

which can be solved for r_L once the characteristic acceleration $\overline{a}_c$ is derived from Eq. (12). Note that Eq. (19) is in accordance with the results discussed in Ref. [41], if it is assumed that the Sun-[Earth+Moon] system center of mass coincides with that of the Sun, and provided that the E-sail thrust model is updated with the recent results given by Ref. [12].

The effectiveness of the proposed control laws has been analyzed assuming an E-sail-based spacecraft with a nominal characteristic acceleration of $\overline{a}_c = 1\,\mathrm{mm/s^2}$ and a grid electric voltage of $\overline{V} = 25\,\mathrm{kV}$. Using the mathematical model discussed in Ref. [32], such a characteristic acceleration may be reached with a total spacecraft mass $m = 696\,\mathrm{kg}$, a payload mass of 200 kg (about 25% greater than that required by the ACE mission), and an E-sail having $N = 16$ tethers with a length of $L = 19.4\,\mathrm{km}$ each. From Eq. (19), the distance of the L_1-type artificial (collinear) Lagrange point from the Sun is $r_L = 0.9436\,\mathrm{au}$, which is in accordance with the previous hypothesis of r to be on the order of 1 au. Such a value of r_L would guarantee a warning time of more than 5.5 hours, that is, five times greater than that given by the ACE mission.

The total mission time of $T = 10$ years is again divided into legs of about 0.58 days, and the simulations have been conducted with the same procedure described for the heliostationary condition scenario. For a given value of the pair $\{V_{\max},\ V_{\mathrm{st}}\}$, the control strategy effectiveness is quantified by the time variation of the radial error with respect to the nominal position, that is

$$\rho_L(t) \triangleq |r(t) - r_L| \tag{20}$$

Different values of $V_{\max}$ and V_{st} have been considered, and 100 simulations have been conducted for each combination. Table 3 reports the mean and the maximum value of ρ_L obtained from simulation with the control strategy $\mathcal{A}$. The case of $V_{\mathrm{st}} \equiv V_{\max}$ is also included, which corresponds to a power system capable of instantaneously adjusting the grid electric voltage. A very accurate orbit maintenance is possible only

$V_{\max}$ [kV]	V_{st} [kV]	ρ_L [au]		ρ_L/r_L [%]	
		mean	max	mean	max
40	1	0.0228	0.1384	2.418	14.660
	5	0.0168	0.1120	1.781	11.863
	10	0.0144	0.0791	1.526	8.385
	40	0.0167	0.0759	1.774	8.044
60	1	0.0234	0.1510	2.483	16.001
	5	0.0208	0.1342	2.199	14.218
	10	0.0172	0.1084	1.821	11.480
	60	0.0107	0.0391	1.131	4.143
80	1	0.0226	0.1539	2.399	16.306
	5	0.0188	0.1410	1.994	14.941
	10	0.0175	0.1087	1.850	11.519
	80	0.0095	0.0294	1.008	3.119
no control		0.0274	0.1193	2.899	8.071

Table 3: Results of the simulations for the artificial Lagrange point maintenance (control strategy $\mathcal{A}$).

for large values of both $V_{\max}$ and V_{st}, when the maximum radial error is about 3% of r_L. This aspect could constitute a technological challenge for future E-sail missions, since when the constraints on $V_{\max}$ and V_{st} are relaxed, the capability for the spacecraft to track the nominal trajectory tends to increase.

Using the same values of $V_{\max}$ and V_{st} as those of Tab. 3, simulations have been conducted also for the control strategy $\mathcal{B}$, considering different values of the tolerance $\epsilon \in \{0,\ 0.01\}$, but the results are omitted here for the sake of conciseness, because the performance of control law $\mathcal{B}$ is significantly worse than that of control law $\mathcal{A}$ in this scenario.

5. Conclusions

A statistical model of the solar wind dynamic pressure has been proposed and used to perform a generalized polynomial chaos-based analysis of the impact of its variability on the E-sail performance. The simulation results about the spacecraft interplanetary trajectory, demonstrate the necessity of a control system capable of adjusting the grid electric voltage in response to in-situ measurements of the solar wind physical characteristics.

Two control laws have been discussed, based on the measurements of the instantaneous dynamic pressure and on instantaneous heliocentric distance, respectively. Both algorithms have been simulated in two advanced mission scenarios, that is, the generation of a heliostationary condition and an artificial Lagrange point maintenance. The control strategy based on the plasma pressure measurements shows a significantly better performance, but the results highlight that both a large maximum grid electric voltage and the capability of quickly adjusting the voltage are advisable, when an accurate thrust modulation is required. A future and more in-depth analysis of control laws should also account for a possible constraint on the power consumption of the E-sail electron gun.

A natural extension of this work consists in analyzing the impact of the solar wind variability in a classical interplanetary rendezvous in which the sail attitude varies continuously in order to obtain the required thrust vector. In that case, a change in nominal characteristic acceleration would affect the (optimal) control law, especially when the actual position of the initial and target planet (or celestial body) is considered during the preliminary mission design. The proposed mathematical model can also be applied to a more advanced mission scenario, such as a flight towards a nearby star system (or the Sun's gravitational lens whose distance is about 550 au), in which the E-sail propulsion system is used to decelerate the spacecraft through the interaction with the interstellar wind.

Acknowledgements

The authors wish to thank Dr. Giovanni Vulpetti for his precious advice. Constructive remarks by the anonymous reviewers are gratefully acknowledged.

Conflict of interest statement

The authors declared that they have no conflicts of interest to this work.

References

[1] P. Janhunen, Electric sail for spacecraft propulsion, Journal of Propulsion and Power 20 (4) (2004) 763–764, doi: 10.2514/1.8580.

[2] P. Janhunen, et al., Electric solar wind sail: Towards test missions, Review of Scientific Instruments 81 (11) (2010) 111301–1–111301–11, doi: 10.1063/1.3514548.

[3] S. Merikallio, P. Janhunen, The electric solar wind sail (E-sail): Propulsion innovation for solar system travel, Bridge 48 (1) (2018) 28–32 .

[4] L. Niccolai, A. A. Quarta, G. Mengali, Electric sail-based displaced orbits with refined thrust model, Proceedings of the Institution of Mechanical Engineers, Part G: Journal of Aerospace Engineering 232 (3) (2017) 423–432, doi: 10.1177/0954410016679195.

[5] L. Niccolai, A. A. Quarta, G. Mengali, Electric sail elliptic displaced orbits with advanced thrust model, Acta Astronautica 138 (2017) 503–511, doi: 10.1016/j.actaastro.2016.10.036.

[6] G. Vulpetti, C. Circi, T. Pino, Coronal mass ejection early-warning mission by a solar-photon sailcraft, Acta Astronautica 140 (2017) 113–125, doi: 10.1016/j.actaastro.2017.07.042.

[7] O. Khurshid, T. Tikka, J. Praks, M. Hallikainen, Accomodating the plasma brake experiment on-board the Aalto-1 satellite, Proceedings of the Estonian Academy of Sciences 63 (2S) (2014) 258–266, doi: 10.3176/proc.2014.2S.07.

[8] P. Janhunen, Electrostatic plasma brake for deorbiting a satellite, Journal of Propulsion and Power 26 (2) (2010) 370–372, doi: 10.2514/1.47537.

[9] L. Orsini, L. Niccolai, G. Mengali, A. A. Quarta, Plasma brake model for preliminary mission analysis, Acta Astronautica 144 (2018) 297–304, doi: 10.1016/j.actaastro.2017.12.048.

[10] P. K. Toivanen, P. Janhunen, Spin plane control and thrust vectoring of electric solar wind sail, Journal of Propulsion and Power 29 (1) (2013) 178–285, doi: 10.2514/1.B34330.

[11] K. Yamaguchi, H. Yamakawa, Study on orbital maneuvers for electric sail with on-off thrust control, Aerospace Technology Japan, the Japan Society for Aeronautical and Space Sciences 12 (2013) 79–88, doi: 10.2322/astj.12.79.

[12] M. Huo, G. Mengali, A. A. Quarta, Electric sail thrust model from a geometrical perspective, Journal of Guidance, Control, and Dynamics 41 (3) (2018) 734–740, doi: 10.2514/1.G003169.
[13] M. Bassetto, G. Mengali, A. A. Quarta, Thrust and torque vector characteristics of axially-symmetric E-sail, Acta Astronautica 146 (2018) 134–143, doi: 10.1016/j.actaastro.2018.02.035.
[14] L. Gallana, F. Fraternale, M. Iovieno, S. M. Fosson, E. Magli, M. Opher, J. D. Richardson, D. Tordella, Voyager 2 solar plasma and magnetic field spectral analysis for intermedate data sparsity, Journal of Geophysical Research: Space Physics 121 (5) (2016) 3905–3919, doi: 10.1002/2015JA021830.
[15] J. L. Phillips, S. J. Bame, A. Barnes, et al., Ulysses solar wind plasma observations from pole to pole, Geophysical Research Letters 22 (23) (1995) 3301–3304, doi: 10.1029/95GL03094.
[16] E. C. Stone, A. M. Frandsen, R. A. Mewaldt, E. R. Christian, D. Margolies, J. F. Ormes, F. Snow, The Advanced Composition Explorer, Space Science Reviews 86 (1–4) (1998) 1–22 .
[17] G. Vulpetti, A critical review on the viability of a space propulsion based on the solar wind momentum flux, Acta Astronautica 32 (9) (1994) 641–644, doi: 10.1016/0094-5765(94)90074-4.
[18] N. Meyer-Vernet, Basics of the Solar Wind, Cambridge University Press, 2007, Ch. 6, pp. 291–333.
[19] G. Vulpetti, Fast Solar Sailing - Astrodynamics of Special Sailcraft Trajectories, Springer, 2013, Ch. 3, pp. 65–92.
[20] G. Vulpetti, L. Johnson, G. Matloff, Solar Sails - A Novel Approach to Interplanetary Travel, 2nd Edition, Springer Praxis, 2014, Ch. 6, pp. 61–66.
[21] P. K. Toivanen, P. Janhunen, Electric sailing under observed solar wind conditions, Astrophysics and Space Science Transactions 5 (1) (2009) 61–69, doi: 10.5194/astra-5-61-2009.
[22] P. K. Toivanen, P. Janhunen, J. Envall, S. Merikallio, Electric solar wind sail control and navigation, in: 1st International Academy of Astronautics Conference on Dynamics and Control of Space Systems, DyCoSS 2012, Porto (Portugal), 2012, paper IAA-AAS-DyCoSS1-03-10.
[23] Y. Wang, B. Bian, Trajectory tracking control of electric sail with input uncertainty and saturation constraint, Transactions of the Institute of Measurement and Control 39 (7) (2017) 1007–1016, doi: 10.1177/0142331215625771.
[24] Y. Luo, Z. Yang, A review of uncertainty propagation in orbital mechanics, Progress in Aerospace Sciences 89 (2017) 23–39, doi: 10.1016/j.paerosci.2016.12.002.
[25] D. Xiu, G. E. Karniadakis, The Wiener–Askey Polynomial Chaos for stochastic differential equations, SIAM J. Sci. Comput. 24 (2) (2003) 619–644, doi: 10.1137/S1064827501387826.
[26] Y. Matsuno, T. Tsuchiya, J. Wei, I. Hwang, N. Matayoshi, Stochastic optimal control for aircraft conflict resolution under wind uncertainty, Aerospace Science and Technology 43 (2015) 77–88, doi: 10.1016/j.ast.2015.02.018.
[27] G. Mengali, A. A. Quarta, P. Janhunen, Electric sail performance analysis, Journal of Spacecraft and Rockets 45 (1) (2008) 122–129, doi: 10.2514/1.31769.
[28] A. A. Quarta, G. Mengali, Minimum-time trajectories of electric sail with advanced thrust model, Aerospace Science and Technology 55 (2016) 419–430, doi: 10.1016/j.ast.2016.06.020.
[29] L. Niccolai, A. A. Quarta, G. Mengali, Two-dimensional heliocentric dynamics approximation of an electric sail with fixed attitude, Aerospace Science and Technology 71 (2017) 441–446, doi: 10.1016/j.ast.2017.09.045.
[30] P. K. Toivanen, P. Janhunen, Thrust vectoring of an electric sail with a realistic sail shape, Acta Astronautica 131 (2017) 145–151, doi: 10.1016/j.actaastro.2016.11.027.
[31] J. M. Sokół, M. Bzowski, M. Tokumaru, K. Fujiki, D. J. McComas, Heliolatitude and time variations of solar wind structure from in situ measurements and interplanetary scintillation observations, Solar Physics 285 (1-2) (2013) 167–200, doi: 10.1007/s11207-012-9993-9.
[32] P. Janhunen, A. A. Quarta, G. Mengali, Electric solar wind sail mass budget model, Geoscientific Instrumentation, Methods and Data Systems 2 (1) (2013) 85–95, doi: 10.5194/gi-2-85-2013.
[33] P. K. Toivanen, P. Janhunen, J. Envall, Electric sail control mode for amplified transverse thrust, Acta Astronautica 106 (2015) 111–119, doi: 10.1016/j.actaastro.2014.10.031.
[34] G. Mengali, A. A. Quarta, Optimal heliostationary missions of high-performance sailcraft, Acta Astronautica 60 (8-9) (2007) 676–683, doi: 10.1016/j.actaastro.2006.07.018.
[35] M. Bassetto, G. Mengali, A. A. Quarta, Stability and control of spinning E-sail in heliostationary orbit, Submitted. Journal of Guidance, Control, and Dynamics .
[36] A. A. Quarta, G. Mengali, Solar sail capabilities to reach elliptic rectilinear orbits, Journal of Guidance, Control, and Dynamics 34 (3) (2011) 923–926, doi: 10.2514/1.51638.
[37] A. A. Quarta, G. Mengali, Optimal solar sail transfer to linear trajectories, Acta Astronautica 82 (2) (2013) 189–196, doi: 10.1016/j.actaastro.2012.03.005.
[38] L. F. Shampine, M. K. Gordon, Computer Solution of Ordinary Differential Equations: The Initial Value Problem, W. H. Freeman, San Francisco, 1975, Ch. 10, ISBN: 978-0716704614.
[39] L. F. Shampine, M. W. Reichelt, The MATLAB ODE suite, SIAM Journal on Scientific Computing 18 (1) (1997) 1–22, doi: 10.1137/S1064827594276424.
[40] G. Aliasi, G. Mengali, A. A. Quarta, Artificial equilibrium points for a generalized sail in the circular restricted three-body problem, Celestial Mechanics and Dynamical Astronomy 110 (4) (2011) 343–368, doi: 10.1007/s10569-011-9366-y.
[41] G. Aliasi, G. Mengali, A. A. Quarta, Artificial equilibrium points for an electric sail with constant attitude, Journal of Spacecraft and Rockets 50 (6) (2013) 1295–1298, doi: 10.2514/1.A32540.
[42] G. Aliasi, G. Mengali, A. A. Quarta, Artificial periodic orbits around L1-type equilibrium points for a generalized sail, Journal of Guidance, Control, and Dynamics 38 (9) (2015) 1847–1852, doi: 10.2514/1.G000904.